Seismic processing of numerical EM data

John W. Neese and Leon Thomsen, University of Houston*

Summary

The traditional methods for acquiring and processing CSEM data are very different from those for seismic data. But Thomsen et al (2007, 09), Strack, et al (2008), and Thomsen (2014) argue that the deep connection between electromagnetics and seismics suggests that many *seismic* processing methods of acquisition and processing could be useful for *EM* data. As examples of this principle, we present here results of semblance analysis, *f-k* filtering, and modified Radon transformation of a commonly-used 1-D numerical EM model, with an impulsive source. Using these seismic methods, we both detect and quantitatively characterize the reservoir, without mathematical inversion.

Introduction

Thomsen, et al (2009) and Thomsen (2014) make the following points concerning the deep connection between EM and seismics, *despite* the fact that EM follows the diffusion equation, whereas anelastic seismics follows the wave equation (see those works for details and references):

1) Both wave types may be described as a Fourier superposition of plane waves.
2) The wave vectors in both cases have both real and imaginary parts, which lead to dispersive, attenuative propagation.
3) Hence, although seismic dispersion and attenuation are weak, whereas EM dispersion and attenuation are strong, *any* seismic processing algorithm which does *not* assume weak dispersion and attenuation is, in principle, applicable to EM data processing.
4) In particular, EM data may be directly *imaged*, using seismic-like techniques, *rather than* mathematically *inverted* for subsurface physical properties; this has various advantages, including less sensitivity to source strength and orientation.
5) In both seismic and EM cases, since the signal from the subsurface is weak, it is best to detect it *without* a concurrent active source. Hence, EM data should (optimally) be Impulsive-Source (ISEM), rather than Continuous-Source (CSEM) data. Further, the EM receivers should not be spatially aliased.
6) The phase velocities of EM waves at low frequencies (~1 Hz) are *comparable* to seismic velocities (several km/s), so that seismic-style acquisition parameters are feasible, and moveout of the EM signal is a primary observable.
7) The further offsets in both cases are weaker, so to compare with nearer offsets, it is convenient to apply seismic-style amplification, such as trace normalization, prior to processing.

To illustrate these points, we present here the results of seismic-style processing that exploits the moveout of synthetic 1-D ISEM data:

a) Velocity (semblance) analysis and stacking
b) *f-k* transform and filtering
c) Conventional and modified Radon transformation

Of these, we find that the Radon transform is the most useful for detecting the presence of hydrocarbons in the subsurface, and that a modification of the Radon transform (defined below) actually makes useful images of the subsurface values of electrical resistivity (the physical parameter which controls the velocity of EM waves in the subsurface).

The canonical model and numerical simulations

Our 1-D "canonical model" (Constable and Weiss, 2006) is comprised of a semi-infinite half space of air (resistivity ρ=10^6 Ohm-m), over ocean (ρ=0.3) 1 km deep, over sediments (ρ=1.0) 1 km deep, over reservoir rock (ρ=100.0) 100 m thick, over a semi-infinite half space of sediments. The source is an impulsive in-line horizontal electric current dipole at 50 m above the seafloor, with negative polarity. The receivers are 200 in-line horizontal electric dipole antennae, stationed from 50 m to 10 km offset (50 m intervals) along the ocean bottom. A second model (the "shallow-water model") was identical except for an ocean depth of 500 m. The 10 second listen time is computed at a 2 millisecond sample rate. Note the similarity to seismic acquisition geometry. (Decimation of such numerical data establishes that larger receiver spacing and longer sampling intervals may often be acceptable.)

Forward simulations were run using a MATLAB fast Hankel transform code (Key, 2012) employing 101 terms in the Hankel expansion. Seismic processing was done using the SU seismic processing package (Stockwell and Cohen, 2008), and making use of UNIX scripts published in the SEG seismic processing primer (Forel, et al, 2005). The forward modeling is very similar to that of Strack, et al (2008).

ISEM moveout

In Figure 1, the first four images show simulations starting with a) whole space seawater, and progressively building the canonical model by adding in b) sediment, c) air, and d)

DOI http://dx.doi.org/10.1190/segam2014-1238.1

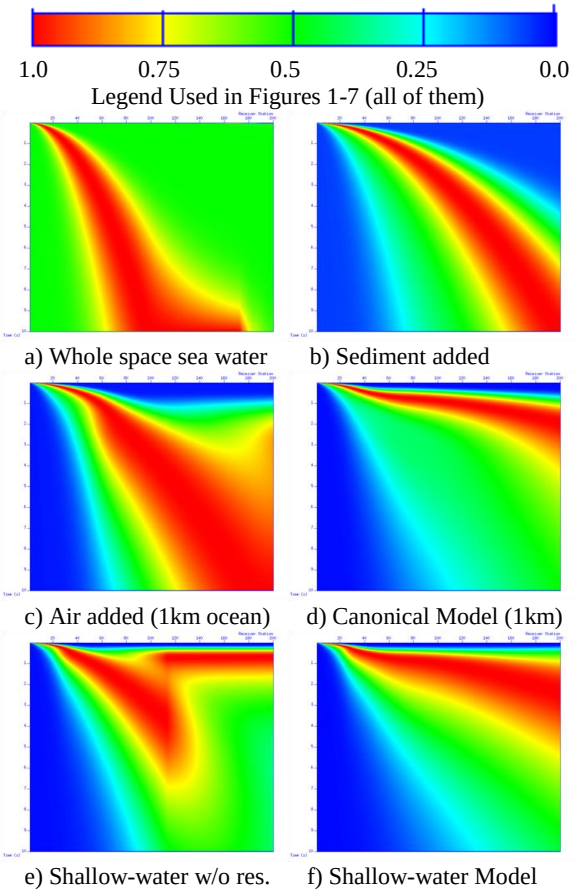

Figure 1: Normalized Simulations:
10s down, 10 km across

the reservoir. Parts e) and f) are the equivalent of c) and d), but for the shallow-water model. In keeping with seismic practice, traces are plotted against receiver offset, with each trace normalized to unit maximum amplitude, which makes the weak far-offset signal visible (seismic-style) without computation of apparent resistivity (EM-style). Each element possesses a distinctive moveou,t similar to seismic data, but with significant dispersion.

The low-frequency EM body-wave phase slowness (inverse of velocity) for a homogeneous non-magnetic isotropic body has real part given by (Thomsen, 2014):

$$s = \sqrt{\frac{\mu_0}{2\rho\omega}} \qquad (1)$$

where μ_0 is the magnetic permeability of free space. This formula, along with the analysis of Thomsen (2014) for a body wave at an interface, leads to the following description of these plots. The "air wave" propagates slowly up through the seawater, refracts horizontally through the air at the speed of light, then propagates slowly back down to the receivers. This is evident in the early arrival at far offsets, which is obvious in part c), and even more obvious in part e), with its shallower water layer.

Similarly the reservoir wave propagates slowly down to the reservoir though the sediments, refracts rapidly through the reservoir, then propagates slowly back up to the receivers.

The above behavior suggests that identifying the reservoir by means of conventional seismic processing tools via the different *moveouts* of various modes, rather than their amplitudes, may be feasible (Thomsen, et al. 2009). Because the air wave is excited impulsively, rather than continuously, it arrives late and fast, and is easily distinguished from the signal (Thomsen, et al, 2009).

Frequency content

Figure 2 shows a frequency spectrum (SUSPECFX) for the canonical model, Figure 1d. Notable is the loss of high frequency with offset, despite the trace normalization. Further, note that the refracted waves (air, reservoir) re-introduce higher frequency content at the longer offsets.

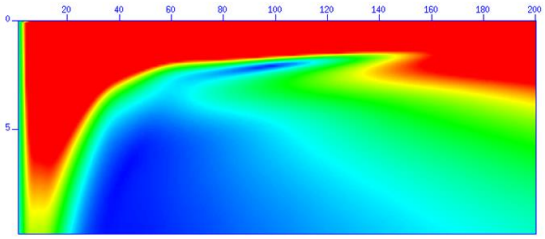

Figure 2: Frequency Content: Canonical Model
(10Hz down, 10km across)

Semblance analysis

Semblance was computed with the SUVELAN program embedded in a UNIX script adapted from iva.sh (Forel, et al, 2005). Figure 3 shows output from the script for the canonical model with and without the reservoir. Velocities run from 500 m/s up to 38000 m/s in 150 increments.

Overlaid on the semblance plots are limited-range (1-10km) Constant Velocity CMP Stacks computed at 3, 10, 17, 24, and 31 km/s. One sees notable differences in the semblance plots and stacks; differences which suggest the ability to detect the reservoir on the basis of its moveout, rather than its amplitude (as in CSEM). Note that the detection does not rely upon forming the numerical difference between on-reservoir and off-reservoir datasets.

DOI http://dx.doi.org/10.1190/segam2014-1238.1

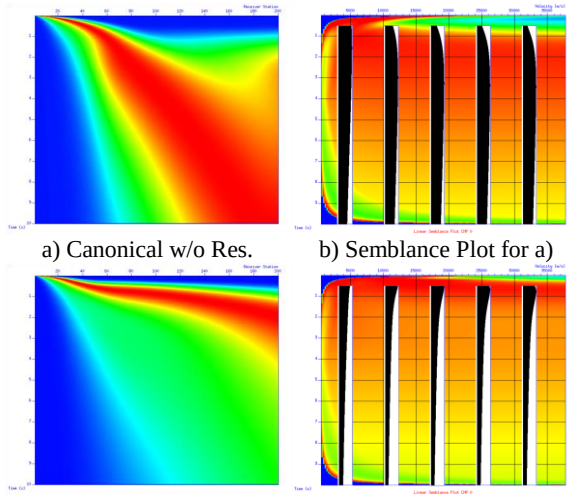

a) Canonical w/o Res. b) Semblance Plot for a)

c) Canonical Model d) Semblance Plot for c)

Figure 3: Simulations on left: 10s down, 10 km across; Semblance Plots on right: 10 s down, 38000 m/s across

However, the plots do not appear to be useful for picking stacking velocities; this is presumably because the EM velocities are so dispersive.

***f-k* analysis**

The UNIX script ifk.sh (Forel, et al, 2005) was adapted to study the *f-k* amplitude spectrum produced by SUSPECFK. Figure 4 shows output from the script, for the simulations with and without reservoir. It is remarkable how similar are the two *f-k* plots, given the differences in the input data. It is not clear from the *f-k* plots what strategy would be promising for identifying the reservoir.

Radon transform

Radon transforms (SURADON) for the canonical model are presented in Figure 5. In the absence of dispersion, an arrival refracted along the reservoir would appear as a straight *line* in time-offset space. We restrict ourselves to linear "tau-p" transforms here, so that the refracted reservoir arrival should, in the absence of dispersion, approximate a *point* in the tau-p domain. Dispersion smears this point considerably, as shown in Figure 5d.

Following experiential guidelines (Yilmaz, 2001), the number of p values was set equal to the number of offsets (200), and the p range was chosen to bracket slownesses of interest: (.03-.27) s/km (33-4 km/s). Strong energy is present at about 0.07 s/km (14 km/s) when the reservoir is present, and absent when the reservoir is absent; this

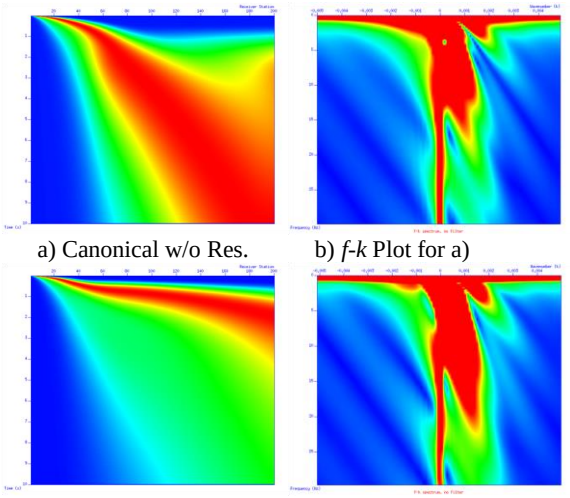

a) Canonical w/o Res. b) *f-k* Plot for a)

c) Canonical Model d) *f-k* Plot for c)

Figure 4: Simulations on left: 10s down, 10 km across; *f-k* plots on right: 30 Hz down, -0.005 to 0.005 m^{-1} across

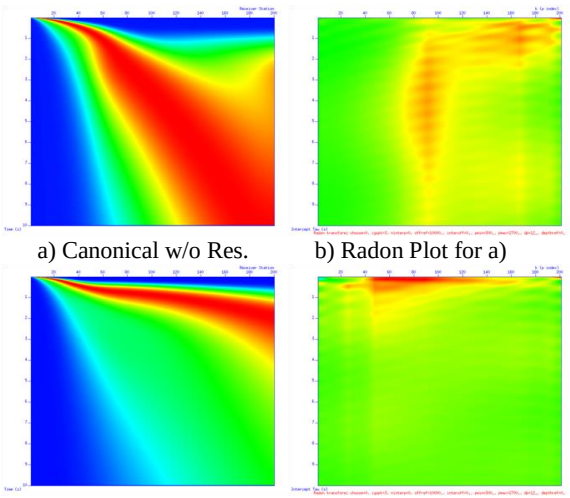

a) Canonical w/o Res. b) Radon Plot for a)

c) Canonical Model d) Radon Plot for c)

Figure 5: Simulations on left: 10s down, 10 km across; Radon Plots on right: 10 s down, 1 s/m across

corresponds to the phase velocity of a wave refracting along the reservoir (ρ=100.0 Ohm-m) at 0.2 Hz.

The result is actually less clear for the shallow-water model, Figure 6. This shows that the Radon transform, as implemented in SURADON, can be frustrated by air wave interference. Refinements to the algorithm can presumably solve this problem, since the differences are clear in the

DOI http://dx.doi.org/10.1190/segam2014-1238.1

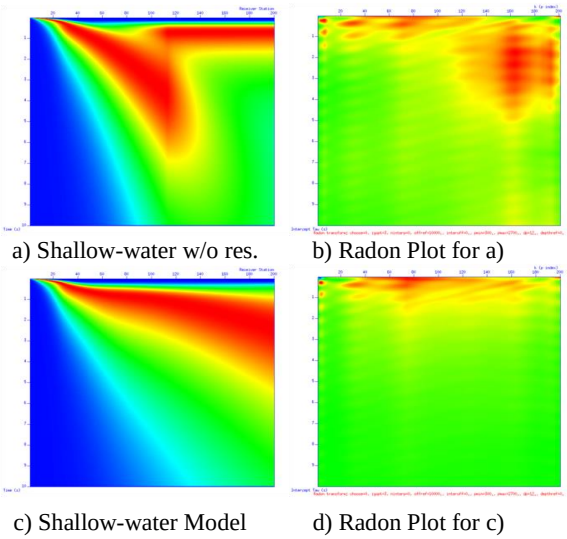

a) Shallow-water w/o res. b) Radon Plot for a)

c) Shallow-water Model d) Radon Plot for c)

Figure 6: Simulations on left: 10s down, 10 km across; Radon Plots on right: 10 s down, 1 s/m across

time-offset domain.

A modified Radon transform for resistivity itself

The SURADON code (Anderson, 1993) computes the forward Radon transform using a least squares representation of the transform in the frequency domain. This method is particularly well-suited to EM, because it enables a natural allowance for the high dispersion of EM waves. After converting the data from the time domain to the frequency domain, SURADON computes slowness, one frequency at a time. It can therefore be converted to the square root of conductivity (inverse of resistivity) at each frequency, simply by dividing each slowness by $\sqrt{(\mu_0/2\omega)}$ (cf. Eqn. 1). Upon conversion back into the time domain, the output is intercept τ versus the square root of conductivity $\sqrt{(1/\rho)}$.

In Figures 7 b) and d), this transform is called "emRadon" and is computed over 200 values of $\sqrt{(1/\rho)}$, from .0036 to 0.72 $\sqrt{}$(Siemens/m). Strong energy between .1-.3 $\sqrt{}$(S/m) (corresponding to ρ=100-30 Ohm-m) is present with the reservoir (7d) (at times less than 1 second), and absent without it (7b). This constitutes a crude image (in time) of the reservoir, in this 1D model.

Parts e) and f) of the figure show the inverse transforms of b) and d). Part e) is a poor recovery of a) because the $\sqrt{(1/\rho)}$ range is inappropriate for this model with no reservoir. On the other hand, part f) recovers the canonical model remarkably well.

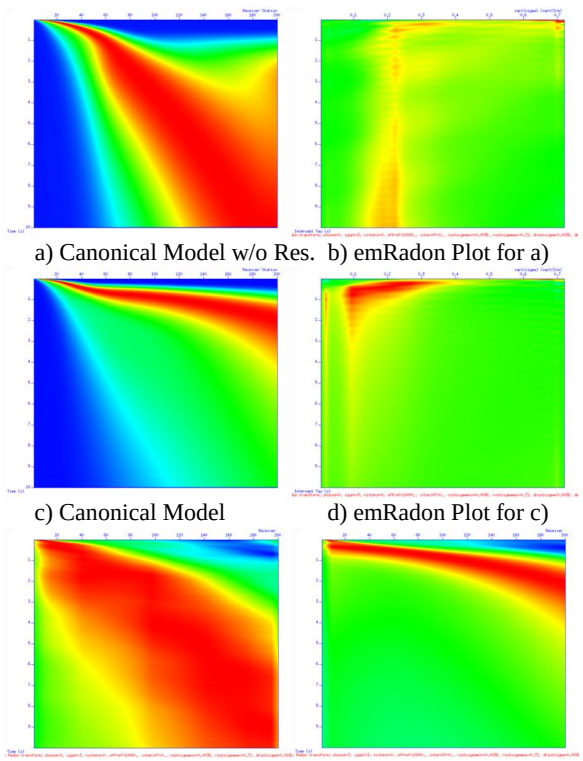

a) Canonical Model w/o Res. b) emRadon Plot for a)

c) Canonical Model d) emRadon Plot for c)

e) Inverse emRadon of b) f) Inverse emRadon of d)

Figure 7: Simulations a), c): 10 s down, 10 km across; emRadon plots b), d): 10 s down, 0.072 $\sqrt{}$(S/m) across; Inverse emRadon plots e), f): 10 s down 10 km across

Conclusions

We have presented the results of seismic-style processing which exploits the moveout of synthetic 1-D EM data:

a) Velocity (semblance) analysis and stacking
b) *f-k* transform and filtering
c) Conventional and modified Radon transforms

We find that the Radon transform is the most useful for detecting hydrocarbons in the subsurface, and that a modification of the Radon transform actually makes useful images of the subsurface values of electrical resistivity. Presumably, modifications and extensions of these simple workflows will be necessary to illustrate these theoretical principles in more complex contexts.

Acknowledgements

We thank Kerry Key for pointing us to his simulation software, John Anderson for help in understanding his SU Radon module, and John Stockwell for help in implementing the SU seismic processing package.

DOI http://dx.doi.org/10.1190/segam2014-1238.1

http://dx.doi.org/10.1190/segam2014-1238.1

EDITED REFERENCES

Note: This reference list is a copy-edited version of the reference list submitted by the author. Reference lists for the 2014 SEG Technical Program Expanded Abstracts have been copy edited so that references provided with the online metadata for each paper will achieve a high degree of linking to cited sources that appear on the Web.

REFERENCES

Anderson, J. E., 1993. Parabolic and linear 2D tau-p transforms using the generalized radon transform: Center for Wave Phenomena, Colorado School of Mines, CWP-137, 109–120.

Constable, S., and C. J. Weiss, 2006, Mapping thin resistors and hydrocarbons with marine EM methods: Insights from 1D modeling: Geophysics, **71**, no. 2, G43–G51, http://dx.doi.org/10.1190/1.2187748.

Forel, D., T. Benz, and W. D. Pennington, 2005, Seismic data processing with Seismic Un*x, a 2D seismic data processing primer: SEG Course Notes Series 12.

Key, K., 2012, Is the fast Hankel transform faster than quadrature?: Geophysics, **77**, no. 3, F21–F30.

Stockwell, J. W., and J K. Cohen, 2008, The new SU user's manual version 4.0: Colorado School of Mines Center for Wave Phenomena.

Strack, K., N. Allegar, and S. Ellingsrun, 2008, Marine time domain CSEM: An emerging technology: 78th Annual International Meeting, SEG, Expanded Abstracts, 78,

Thomsen, L., D. Meaux, S. Li, C. Weiss, A. Sharma, N. Allegar, and K. Strack, 2007, From deep into shallow water: Recent advances and the road ahead: 77th Annual International Meeting, SEG, Expanded Abstracts, 77.

Thomsen, L., 2014. Electromagnetics and seismics: The deep connections: Presented at the 84th Annual International Meeting, SEG.

Thomsen, L. A., N. C. Allegar, J. A. Dellinger, P. Jilek, D. T. Johnson, and G. Xia, 2009, System and method for using time-distance characteristics in acquisition, processing, and imaging of t-CSEM data: U. S. Patent 7,502,690; 7941273.

Yilmaz, O., 2001, Seismic data analysis: Processing, inversion, and interpretation of seismic data: SEG.